ACS APPLIED MATERIALS & INTERFACES

Research Article

www.acsami.org

Effects of Gold-Nanoparticle Surface and Vertical Coverage by Conducting Polymer between Indium Tin Oxide and the Hole Transport Layer on Organic Light-Emitting Diodes

Sung Hyun Kim,[†] Tae-Sung Bae,[‡] Wooseok Heo,[§] Taiha Joo,[§] Kyung-Deok Song,[∥] Hong-Gyu Park,[∥] and Seung yoon Ryu*,[⊥]

[†]Department of Chemistry, College of Natural Sciences, Seoul National University, Seoul 151-747, Republic of Korea

[‡]Jeonju Center, Korea Basic Science Institute (KBSI), Analysis & Researcher Division, 634-18 Geumam-dong, Deokjin-gu, Jeonju-si, Jeollabuk-do 561-756, Republic of Korea

[§]Department of Chemistry, Pohang University of Science and Technology (POSTECH), 77 Cheongam-Ro, Nam-Gu, Pohang, Gyeongbuk 790-784, Republic of Korea

[∥]Department of Physics, Korea University, 145 Anam-ro, Seongbuk-gu, Seoul, 136-701, Republic of Korea

[⊥]Department of Information Communication & Display Engineering, Division of Mechanical and ICT Convergence Engineering, Sunmoon University, 221, Sunmoon-ro, Tangjeong-myeon, Asan, Chungnam 336-708, Republic of Korea

Supporting Information

ABSTRACT: The effect of varying degrees of surface and vertical coverage of gold nanoparticles (Au-NPs) by poly-(styrenesulfonate)-doped poly(3,4-ethylenedioxythiophene) (PEDOT:PSS), which was used as a capping layer between indium tin oxide (ITO) and a hole transport layer (HTL) on small-molecule fluorescent organic light-emitting diodes (OLEDs), was systemically investigated. With respect to the Au-NP loading amount and size, the resultant current densities influenced the charge balance and, therefore, the OLED device performance. When the capping layer consisted of ITO/Au-NPs/PEDOT:PSS+Au-NPs, superior device performance was obtained with 10-nm Au-NPs through increased surface coverage in comparison to other Au-NP PEDOT:PSS coverage conditions. Furthermore, the Au-NP size determined the vertical coverage of the capping layer. The current densities of OLEDs containing small Au-NPs (less than 30 nm, small vertical coverage) covered by PEDOT:PSS decreased because of the suppression of the hole carriers by the Au-NP trapping sites. However, the current densities of the devices with large Au-NPs (over 30 nm, large vertical coverage) increased. The increased electromagnetic fields observed around relatively large Au-NPs under electrical bias were attributed to increased current densities in the OLEDs, as confirmed by the finite-difference time-domain simulation. These results show that the coverage conditions of the Au-NPs by the PEDOT:PSS clearly influenced the OLED current density and efficiency.

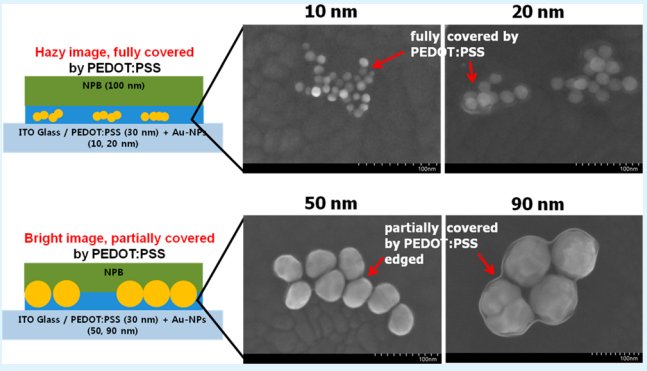

KEYWORDS: *gold nanoparticles, organic light-emitting diodes, conducting polymer, surface and vertical coverage, charge balance, surface plasmonic resonance effect*

INTRODUCTION

Reduced power consumption is one of the main goals that should be achieved to realize the mass production of organic light-emitting diodes (OLEDs).[1−8] Thus, considerable attention has been paid to increasing OLED efficiency in order to reduce power consumption. The charge balance between the holes and electrons within these devices is an important factor determining the efficiency.[2,3] In particular, an enhanced hole injection capability is required to overcome the effects of the large injection barrier between the transparent anode and hole transporting layer (HTL).[2−5] Gold nanoparticles (Au-NPs)[1−8] have been introduced as a manner of improving OLED performance through both electrical and optical means, by enhancing the charge balance through management of the hole carrier density[3−6] and strengthening the luminance efficiency via the surface plasmonic resonance (SPR) effect, respectively.[5−10] The most important criterion determining the SPR effect is the optical effect due to the overlap between the Au-NP absorption and the emission of the emitter.[5−10] The coincidence of these two spectra generates resonance between

Received: May 15, 2015
Accepted: June 22, 2015
Published: June 22, 2015

DOI: 10.1021/acsami.5b04248
ACS Appl. Mater. Interfaces 2015, 7, 15031−15041

the surface plasmons (SPs) at the Au-NPs and the radiated light from the emitter, enhancing the electroluminescence (EL).[5−10] The other factor influencing the SPR effect is the distance between the Au-NPs and the emitter, because the number of surface plasmons (SPs) in the vicinity of the metal nanoparticles exponentially decreases as this distance increases.[2−6] The SPR effect can be quite efficient for dipole−dipole coupling between SPs and excitons within a 10-nm distance.

In terms of the charge balance dependency on the hole injection and its effect on the electrical properties (not the SPR optical effect), the surface coverage of the OLED anode, which is controlled by the degree of Au-NP dispersion, has been found to be extremely critical as regards variation of the hole current density,[3−6] although the exact mechanism has not been established. It has been found that, when the Au-NP surface coverage on an indium tin oxide (ITO) anode (with no added poly(styrenesulfonate)-doped poly(3,4-ethylenedioxythiophene) (PEDOT:PSS)) is over 2.1%,[4,5] the hole injection is increased compared to that of a control device without Au-NPs. This enhancement is attributed to the reduction of the potential barrier between the ITO and HTL.[3−6] However, for surface coverage of less than 2.1%, the hole injection was found to be suppressed. This is explained as being due to the fact that Au-NPs capture the hole carriers because of the electrostatic interaction between them;[3−6] however, a deeper understanding of this behavior has not yet been obtained.

Another approach to enhancing the charge balance is through the addition of Au-NPs to a conduction polymer (PEDOT:PSS) on the ITO anode. Although a small number of studies on the effects of introducing Au-NPs to PEDOT:PSS for increased hole injection have been conducted,[1,3,6−8] the effects of varying the degree of vertical coverage of the Au-NPs by the PEDOT:PSS have, to the best of our knowledge, not been studied. Note that, here, we define surface coverage as the lateral distribution depending on the Au-NP density, whereas vertical coverage is dependent on the sizes of the Au-NPs themselves, that is, whether or not the Au-NPs are enclosed within the PEDOT:PSS. Moreover, the surface coverage can be categorized in two ways: Surface coverage without PEDOT:PSS is simply a two-dimensional distribution on the ITO, while that with PEDOT:PSS is a three-dimensional distribution (a small number of stacked layers) within the PEDOT:PSS due to the aggregation of the Au-NPs.[7,8,11,12] Hence, both the PEDOT:PSS thickness and the Au-NP size are quite critical as regards both the surface and vertical coverage, which ultimately affect the device performance.

To apply the SPR effect, Kim et al. have reported that relatively small Au-NPs (∼12 nm in diameter) blended with PEDOT:PSS have been incorporated into transparent anodes in OLEDs.[1] PEDOT:PSS itself has been widely used as an interfacial layer to adjust the hole injection capability of ITO anodes in OLEDs. However, this approach has yielded the disadvantage of a high operating voltage, at over 15 V at 1000 cd/m^2, in spite of a moderately improved efficiency, resulting from relatively low anode sheet resistance compared to those of the examined control devices without Au-NPs. This limited device performance can be explained as being due to a small SPR effect and poor charge balance.

PEDOT:PSS blended with relatively large Au-NPs (40−50 nm)[6,7] or polystyrene-coated Au-NPs (Au@PS NPs) has been used to create a localized SPR effect.[5−10] Further, improved EL has been achieved through the overlap of the Au-NP absorptions and the photoluminescence (PL) spectrum of the emitters, and has been confirmed through examination of the exciton lifetime measured using time-resolved PL spectroscopy.[7] Although the light extraction efficiency due to the incorporation of large Au-NPs close to the emitters (less than 10 nm) was found to be strengthened by the SPR effect, the resultant device performance was relatively low. This was because of a charge imbalance with energy-level mismatch that was due to the absence of transporting materials and the hindrance of charge transport.[7] In addition, these reported results did not indicate a clear relationship between the SPR effect and the carrier trapping at the Au-NPs in terms of the hole injection capability and the corresponding charge balance. The correlation between the coverage of a capping layer on the ITO anode containing Au-NPs of different sizes and at varying positions and the resultant OLED performance is, therefore, far from being established.

In this study, we examined different devices with varying degrees of surface and vertical coverage of Au-NPs by PEDOT:PSS, which was positioned between ITO and an HTL in fluorescent OLEDs. We correlated the measured device performance with the Au-NP coverage parameters, which were determined by the Au-NP loading amount and size. A 100-nm-thick HTL was used to prevent short circuiting and to eliminate the SPR effect, so that this factor could be neglected as a source of the observed behavior. To gain insight into the role of the Au-NPs in relation to the OLED performance, the hole injection capability and interfacial resistance were investigated by examining the current densities of hole-only devices (HODs) and the impedance of the Cole−Cole plot. A finite-difference time-domain (FDTD) simulation was conducted to verify the local electromagnetic fields around the Au-NPs in the fabricated devices, so as to understand the changes in the current densities in response to variations in the vertical coverage of the Au-NPs in the PEDOT:PSS.

EXPERIMENTAL SECTION

1. PEDOT:PSS with Au-NP sample preparation. Heraeus Clevios P VP AI 4083 PEDOT:PSS (Ossila) and 0.05-mg/mL Au-NPs in aqueous suspension (Sigma-Aldrich) were purchased commercially. Note that all unconjugated gold colloids contain approximately 0.01% $HAuCl_4$ suspended in 0.01% tannic acid with 0.04% trisodium citrate, 0.26 mM potassium carbonate, and 0.02% sodium azide as a preservative.

To investigate the effects of varying degrees of Au-NP surface coverage, 10-nm Au-NPs were selected, with monodispersity being confirmed by the manufacturer. For device II (described below), PEDOT:PSS blended with isopropanol (IPA) without 10-nm Au-NPs ((PEDOT:PSS):IPA = 1:2 by volume) was spin-coated on ITO, to be matched with the total dilution level of the PEDOT:PSS blended with the IPA and Au-NP solution.

To investigate the effects of varying vertical Au-NP formations, 10- (mean particle size: 8.5−12.0 nm), 20- (mean particle size: 18.5−22.5 nm), 50- (mean particle size: 47.5−53.0 nm), and 90-nm Au-NPs (mean particle size: 85.0−95.5 nm) were selected. PEDOT:PSS blended with IPA with Au-NPs of each size ((PEDOT:PSS):IPA:Au-NP = 1:1:1 by volume) was spin-coated on ITO. The IPA was used for film formation.

2. Sample preparation and device fabrication. To construct the OLEDs, ITO glass was initially cleaned with deionized water, acetone, and IPA under sonication at 40 kHz and then subjected to ultraviolet-ozone (UV/O3) treatment, in order to adjust the ITO work function. To deposit the Au-NPs onto the ITO (device I), Au-NPs of ∼10 nm in size and dispersed in IPA (Au-NPs:IPA = 1:2 by volume) were spin-coated at a rotation speed of 3000 rpm. For device II, PEDOT:PSS blended with IPA ((PEDOT:PSS):IPA = 1:2 by volume)

DOI: 10.1021/acsami.5b04248
ACS Appl. Mater. Interfaces 2015, 7, 15031−15041

was spin coated onto the ITO glass. For device III, PEDOT:PSS blended with Au-NPs and IPA ((PEDOT:PSS):IPA:Au-NPs = 1:1:1 by volume) was spin coated onto the ITO glass while, for device IV, PEDOT:PSS blended with Au-NPs and IPA ((PEDOT:PSS):IPA:Au-NPs = 1:1:1 by volume) was spin coated onto ITO glass coated with Au-NPs (Au-NPs:IPA = 1:2 by volume). For device V, Au-NPs with IPA (Au-NPs:IPA = 1:2) were spin coated onto the PEDOT:PSS+Au-NP film ((PEDOT:PSS):IPA:Au-NPs = 1:1:1 by volume), formed on the ITO glass coated with Au-NPs (Au-NPs:IPA = 1:2 by volume). The PEDOT:PSS layer with/without the NPs (devices II–V) was then annealed on a hot plate at 200 °C for 10 min under ambient conditions. The thickness of the capping layer was confirmed to be approximately 30 nm, using spectroscopic ellipsometry (SE). The optical density (OD)[13] was estimated based on the absorption ratio for the capping layer with different Au-NP concentrations, and compared with that of the PEDOT:PSS layer without Au-NPs, as shown in Figure S1 of the Supporting Information.

After the baking process, *N*,*N*-bis(1-naphthyl)-*N*,*N*′-diphenyl-1,1′-biphenyl-4,4′diamine (NPB), 2,3,6,7-tetrahydro-1,1,7,7,-tetramethyl-1*H*,5*H*,11*H*-10(2-benzothiazolyl) quinolizino-[9,9*a*,1*gh*]-coumarin (C545T) 3%-doped tris(8-quinolinolato) aluminum (Alq_3), and Alq_3 were thermally deposited as an HTL (100 nm), an emission layer (EML; 40 nm), and an electron transport layer (ETL; 25 nm), respectively, in a high-vacuum chamber. Finally, a LiF/Al (1 nm/120 nm) layer was deposited via thermal evaporation using a shadow mask with an area of 0.04 cm^2.

3. Device characteristic measurement and optical simulation. The current density–voltage (*J*–*V*) and luminance–voltage (*L*-*V*) characteristics of the fabricated devices, along with their EL spectra, were measured using a Keithley 2400 voltmeter and a PhotoResearch PR-650 spectrometer. Ultrahigh-resolution field-emission scanning electron microscopy (UHR FE-SEM, S-5500, Hitachi, Japan) was also conducted at the KBSI Jeonju Center, for an accelerating voltage of 7 kV.[14,15] The PL lifetime[7] was also measured using the time-correlated single-photon-counting (TCSPC)[16,17] method. Picosecond time-resolved fluorescence experiments were performed through TCSPC. The light source was a home-built cavity-dumped Ti:sapphire oscillator pumped by a frequency-doubled Nd:YVO4 laser (Verdi, Coherent Inc.), and generated 20 fs pulses per 13 ns. The center wavelength of the oscillator output was adjusted to 800 nm and its frequency was doubled using second harmonic generation in a 300-μm-thick β-barium borate (BBO) crystal where the absorption maximum was that of the Alq_3:C545T organic light-emitting layer. The pump pulse power was 0.3 nJ and the fluorescence was collected by a parabolic mirror and detected using a microchannel-plate photomultiplier tube (MCP-PMT; Hamamatsu R3809U-51). The instrumental response function was estimated to be 60 ps (full with at half-maximum; fwhm). Impedance spectroscopy (IS) measurements were conducted using a Novocontrol broadband dielectric spectrometer equipped with a 4-wire impedance test interface in a 2-probe configuration and a Bio-Logic VMP-3 potentiostat, over a range of 1 Hz to 100 MHz with 10-mV oscillation amplitude. The FDTD simulation was performed using home-built software. A laterally polarized monochromatic dipole source was excited at a height of 50 nm from the center of the Au-NPs. A model with one Drude pole and two critical point poles was used to fit the complex permittivity of the Au over a wavelength range of 340–1000 nm.[18] The other materials were assumed as being nondispersive and nondissipative. In simulation, a nonuniform grid method was used to increase the calculation speed. The spatial resolution was 1 nm in the vicinity of the Au-NPs and was gradually increased up to 10 nm outside the fine region. The calculation was iterated over 100 optical periods to reach a steady state, and the electrical field intensity distribution for the final optical period was obtained.

RESULTS AND DISCUSSION

1. Effects of surface coverage of Au-NPs by PEDOT:PSS and Au-NP lateral distribution on device performance. We investigated the effect of varying degrees of surface and vertical coverage of Au-NPs by PEDOT:PSS on device performance, with the surface and vertical coverage being determined by the loading amount and size of the Au-NPs in the PEDOT:PSS. A device structure comprising ITO/a capping layer/NPB/Alq_3:C545T/Alq_3/LiF/Al was constructed, and devices I–V were fabricated with varying characteristics. The capping layers consisted of PEDOT:PSS only (device II), PEDOT:PSS+Au-NPs (device III), and Au-NPs/PEDOT:PSS +Au-NPs (device IV), respectively. For comparison, device I was fabricated with sole Au-NPs spin-coated on the ITO substrate, and device V was composed of Au-NPs/PEDOT:PSS +Au-NPs/Au-NPs. The OD values were 28, 33, and 37 for devices III, IV, and V, respectively, as shown in Figure S1. The schematic device structures are shown in Figures 1 and S2, and

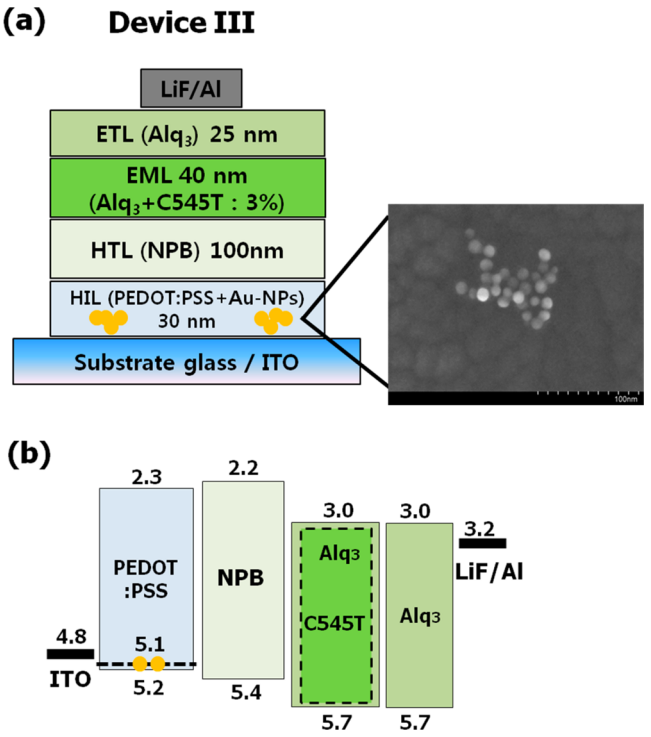

Figure 1. (a) Device III structure with 10-nm Au-NPs in PEDOT:PSS between ITO and NPB HTL. Inset: UHR FE-SEM image of spin-coated (3000 rpm) PEDOT:PSS blended with Au-NPs (~10 nm in size) and IPA ((PEDOT:PSS):Au-NPs in solution:IPA = 1:1:1 by volume) on ITO glass. (b) Corresponding energy band diagram (The yellow spheres represent Au-NPs.).

a corresponding band diagram is shown in Figure 1(b). The Au-NP concentration was constant for all experiments in which the spin-coating process was used; thus, the loading amount of Au-NPs in devices III, IV, and V increased by exact multiples of the spin-coating number in the capping layer.

Note that the use of 2,9-dimethyl-4,7-diphenyl-1,10-phenanthroline (BPhen) material, which has faster electron mobility than Alq_3,[19–21] as an ETL may yield superior device performance because of its superior charge balance and energy band alignment. Therefore, this different device structure will be studied in a future investigation in order to optimize the device performance. The charge balance of holes and electrons in the EML is quite critical to the device performance, and it can be varied by adjusting the carrier mobility at the HTL and ETL.[19–21]

DOI: 10.1021/acsami.5b04248
ACS Appl. Mater. Interfaces 2015, 7, 15031–15041

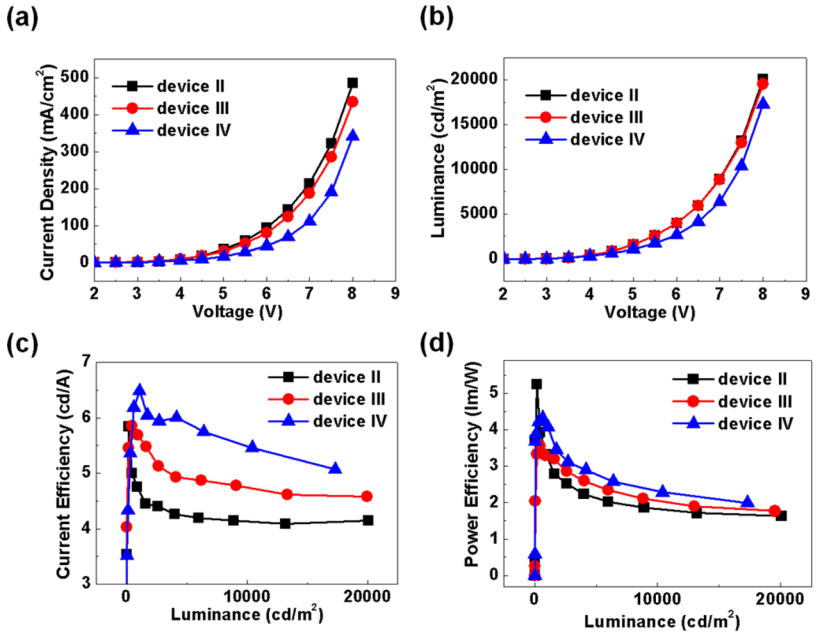

Figure 2. OLED characterization for different Au-NP positions and surface coverages for devices II, III, and IV: (a) Current density vs voltage; (b) luminance vs voltage; (c) current efficiency vs luminance; and (d) power efficiency vs luminance.

To investigate the effects of surface coverage and lateral distribution on the device performance, 10-nm Au-NPs were selected and enclosed in the PEDOT:PSS, in which the Au-NPs were readily aggregated.[7,8,11,12,15] Thus, a small number of diversely formed stacked layers were created in the PEDOT:PSS, according to the specific device configurations given above. The location of the deposited Au-NPs was determined by the stacking order of the device structure. These positions were divided into three categories: below, inside, and above the PEDOT:PSS, as shown in Figures 1 and S2. However, the Au-NPs were primarily aggregated inside the PEDOT:PSS. Therefore, the final formation of the Au-NPs in the PEDOT:PSS is shown as a three-dimensional lateral surface coverage.

In our previous work,[15] Au-NPs located between PEDOT:PSS and tungsten oxide (WO_3) were found to shift the potential barrier from 0.88 to 0.68 eV, which enhanced the hole transport from the WO_3 to the PEDOT:PSS in the device.[15] In this manner, the band alignment between the PEDOT:PSS +Au-NPs and the NPB aided the effective movement of hole carriers between the ITO and the NPB. Figure 1(a, inset) is a micrograph of the aggregated Au-NPs blended with the PEDOT:PSS on ITO glass (device III), obtained using an ultrahigh-resolution field-emission scanning electron microscope (UHR FE-SEM).[14,15] A cluster of Au-NPs can be seen in this case, whereas sole Au-NPs are well-dispersed on the ITO (device I), as shown in Figure S2 inset-(I). With respect to the relationship between the loading amount of the Au-NPs and the spin-coating number for different device structures, the aggregated Au-NPs in the PEDOT:PSS have different morphologies for different devices, as can be seen in Figures 1(a) and S2 insets-(II) and (III). An increase in the Au-NP loading amount is generally accompanied by an increase in the degree of particle aggregation in the PEDOT:PSS, due to electrostatic interaction between each NP and the PEDOT:PSS.[7,8,11,12,15] This aggregated Au-NP formation can interrupt the hole transport and transmute the SPR effect.[3−6]

1.1. OLED device characterization for surface coverage with Au-NPs in PEDOT:PSS. The current density−voltage ($J-V$) and luminance−voltage ($L-V$) characteristics of three OLEDs with Au-NP surface coverage for five differently structured devices are shown in Figures 2(a), 2(b), S3(a), and S3(b). Device I exhibits the poorest current density and luminance results of all the devices apart from device V, which has equally poor performance, as can be seen in Figures S3(a) and (b). In particular, exciton formation almost does not occur, because of reduced current injection via severe carrier capture at the three-dimensional aggregated Au-NPs. As shown in Figure S2 inset-(I), the ITO surface of device I has less than 2.1% Au-NP coverage (device I had 0.15%, as can be seen in Figure S4).[4,5] This poor performance is attributed to the fact that the potential barrier between the Au-NPs and NPB is 0.4 eV.[4,5] In terms of surface coverage, Au-NPs can play the role of trapping sites for carrier capture; besides, from a different standpoint, hole injection is facilitated by the adjustment of the energy band alignment.[3−6] Consequently, the captured carriers at the Au-NP sites in device I under the surface coverage threshold severely break the charge balance in the EML. This result is consistent with previous reports that energy level alignment or trapping sites occur between the capping layer and the anode.[2−6]

In devices III and IV, the Au-NPs are fully enclosed by the PEDOT:PSS, and the hole injection is improved with the assistance of the PEDOT:PSS. This is in comparison with the hole injection exhibited by device I. The current density of device II is higher than those of devices III and IV, because charge carriers are not severely captured at the Au-NP sites.[4−6] Device III (OD = 28) exhibits a slightly decreased current density due to the charge trapping of the Au-NPs in the capping layer,[4−6] while device IV (OD = 33) exhibits significantly less current injection, because of the increase in the Au-NP density and aggregation for charge trapping between the ITO electrode and the NPB layer. Consequently, the device performances deteriorate rapidly in accordance with the OD values over 33. However, the luminance data of devices II and

DOI: 10.1021/acsami.5b04248
ACS Appl. Mater. Interfaces 2015, 7, 15031−15041

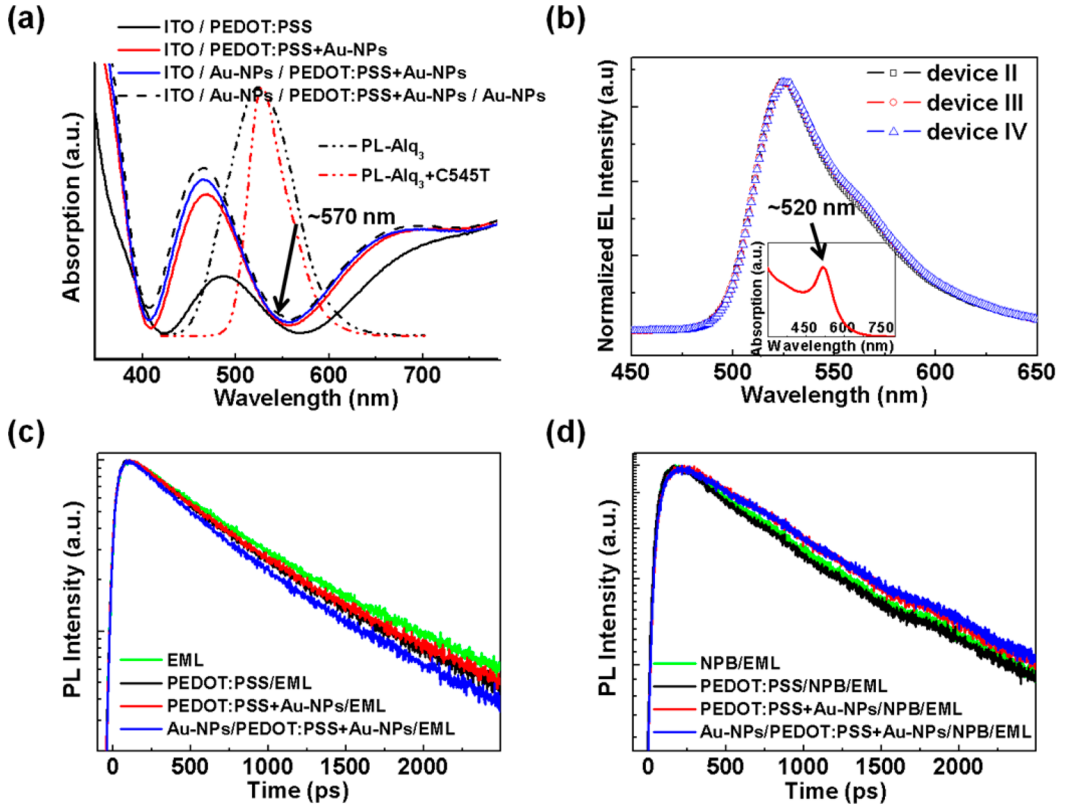

Figure 3. OLED properties depending on different Au-NP positions and degrees of surface coverage: (a) Optical properties, absorption of PEDOT:PSS with Au-NPs and PL intensities of Alq3 and Alq_3+C545T (3%; weight percent); (b) normalized EL intensity (inset: absorption peak of 10-nm Au-NPs in solution); (c) TCSPC data showing changes in PL lifetime without NPB (100 nm); and (d) TCSPC data showing changes in PL lifetime with NPB (100 nm).

III are almost identical, while those of device IV are slightly lower than those of devices II and III, as shown in Figure 2(b). Thus, the current efficiency (cd/A) and power efficiency (lm/W) values of both devices III and IV are higher than those of device II, as shown in Figures 2(c) and (d), respectively. This can be attributed to the fact that the charge balance in the EML is managed by reducing the hole injection caused by the Au NPs. For device IV, luminance of 150 and 20,000 cd/m^2 was obtained at 3.5 and 8 V, respectively. This is a very low operating voltage, in comparison with the operating voltages of over 20 V reported by other research groups.[6,7]

In Figures 2(c) and (d), the current and power efficiency roll-offs of all devices (apart from I and V) are shown. The observed reduction in efficiency roll-off may be due to the trapping sites at the Au-NP locations and the heterojunction contact between the spin-coated PEDOT:PSS and thermally evaporated NPB. The carriers accumulate at the trapping sites and heterogeneous interface, which causes the device operation voltage to increase and eventually leads to deterioration of the efficiency roll-offs. The difference in current efficiencies observed here is larger than the difference in the power efficiencies for all the devices. This can be attributed to the fact that the operating voltage was increased with the increased surface coverage from device II to device IV.

From these results, it was found that the optimized surface coverage of the Au-NPs enclosed by the PEDOT:PSS is beneficial for hole injection, whereas direct contact between the Au-NPs and NPB with low surface coverage and without a PEDOT:PSS capping layer is unfavorable for device efficiency. The latter is due to the resultant heavy carrier accumulation in the Au-NPs that breaks the charge balance.[4−6] In addition, exceeding the threshold of the three-dimensional surface coverage of the Au-NPs aggregated in the PEDOT:PSS almost blocks carrier injection into the device.

1.2. Optical characterization of ultraviolet (UV) absorption data, PL intensities, and EL data for Au-NPs in PEDOT:PSS. The ultraviolet (UV) absorption data, PL intensities, and EL data shown in Figures 3(a) and (b) were used to confirm that the SPR effect had no effect on the device performance in this study. We can infer that the distance between the Au-NPs and the emitters is sufficiently far to prevent the SPR effect, because 100-nm-thick NPB was inserted between the capping layer and the EML. The absorption peak of the pristine Au-NPs in solution shown in Figure 3(b, inset) is at approximately 520 nm.[2−8] Generally, the dielectric environment between the PEDOT:PSS and Au-NPs simultaneously induces either a red shift or a blue shift in UV spectra.[4−8,14,15] In the absorption spectrum of ITO/PEDOT:PSS+Au-NPs film, two main absorption peaks occur in the ranges of 400−550 nm and 550−750 nm, while the PL peak of the Alq_3+C545T EML is in the region of 500−600 nm, as shown in Figure 3(a). The absorption of this film overlaps the PL of the EML in two areas: 500−550 nm and 550−600 nm. However, the PL peak from the emitters in the EML does not overlap the absorption peak of the PEDOT:PSS+Au-NPs on the ITO electrode exactly. This result explains why the EL spectra of the devices with Au-NPs have a slightly enhanced shoulder peak at approximately 570 nm, instead of exhibiting an SPR effect caused by the Au-NPs, as shown in Figures 3(b) and S5.

DOI: 10.1021/acsami.5b04248
ACS Appl. Mater. Interfaces 2015, 7, 15031−15041

The EL intensity of device IV, at approximately 570 nm, is the highest of all the devices. The more Au-NPs that are aggregated in the PEDOT:PSS, the greater the optical enhancement that can occur. Likewise, the current densities are altered by the carrier trapping at the Au-NP sites; thus, a small shift in the recombination zone could be caused by the microcavity effect.[19−21] Note that, although the Au-NPs were enclosed in the PEDOT:PSS, it was not possible to observe a plasmon-derived resonance effect, because little overlap occurred between the absorption of the Au-NPs and the PL of the emitters.

1.3. Analysis of time-correlated single-photon-counting (TCSPC) for Au-NPs in PEDOT:PSS. The PL lifetime[7] was also measured using the time-correlated single-photon-counting (TCSPC)[16,17] method. This was to determine whether plasmon effects in the aggregated 10-nm Au-NPs occurred at the PEDOT:PSS thin film, both with and without the 100-nm-thick NPB, as shown in Figures 3(c) and (d), respectively. Generally, excitons are generated in the EML through excited molecular singlets, exciplexes, and electroplexes. In this study, excitons diffused to the interface between the Au-NPs embedded in either the PEDOT:PSS or NPB, to create diffused transfer (DT) states similar to charge transfer (CT) states in solar cells.[22,23] However, the samples used in the TCSPC analysis could have been affected by DT states and photoexcited excitons, as in solar cells, because the photons were injected into the samples from an external laser source during the TCSPC measurements. Further, fluorescent singlet excitons move quicker than triplets as a result of Förster resonant energy transfer, which can be affected by long-range electrostatic coupling between excited transition dipoles. Thus, polarons are generated by the carriers captured at Au-NPs for holes and C545T dopants for electrons, respectively.[22,23] In the case examined here, the exact correlation between the singlet or triplet diffusion length and a feasible coupling process with the Au-NPs through the NPB blocking layer requires further investigation, which will be conducted in future studies.

Excitons, along with SPs, can be degraded in Au-NP-containing conducting PEDOT:PSS,[6−10] because the dissipation caused by coupling between the SPs at the Au-NPs and the radiated excitons is considerably faster than the spontaneous recombination of the excitons, as shown in Figure 4(a). Therefore, the exciton lifetimes in SP-enhanced devices should be shorter than those in devices without SP enhancement.[7,16,17] The PL lifetimes of the Alq_3+C545T samples with PEDOT:PSS (device II) and PEDOT:PSS+Au-NPs (device III) are slightly shorter than those of the samples without PEDOT:PSS (device I) or with EML only, whereas the sample containing Au-NPs/PEDOT:PSS+Au-NPs (device IV) has a significantly shorter PL lifetime because of the increase in the amount of Au-NPs. However, as shown in Figure 3(d), the PL lifetimes of devices III or IV with 100-nm-thick NPB were slightly longer than those without Au-NPs or with EML only. This can be attributed to our device structure, since the 100-nm-thick NPB layer inserted between the EML and the capping layer blocked the interaction between the SPs on the Au-NPs and the excitons generated in the EML sufficiently, as shown in Figure 4(b).[7] The generated optical enhancement was confirmed through examination of the EL intensity, by examining the light trapping effect caused by the complicated light path created by the aggregated Au-NPs,[11] as shown in Figure S5. Thus, we can infer that Au-NPs may not affect the PL lifetime and device enhancement by the SPR effect if the

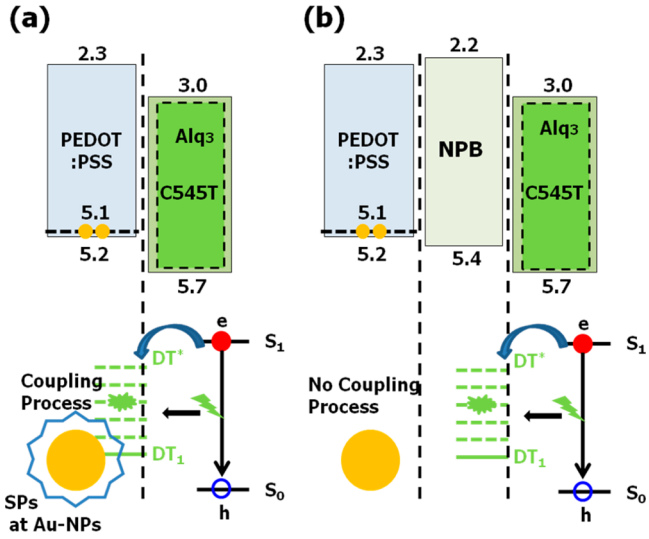

Figure 4. Schematic modeling depending on blocking of 100-nm NPB between SPs around Au-NPs and excitons from emitters: (a) Expected coupling process between SPs around Au-NPs and excitons from emitters without 100-nm NPB; (b) no coupling process between SPs around Au-NPs and excitons from emitters with 100-nm NPB. The DT states are diffused transfer states.

device employs a 100-nm-thick NPB layer. However, the enhancement in the current efficiency in the devices mainly originates from the improved charge balance control rather than from the SPR effect.[6−10]

1.4. Analysis of correlation between hole capture and resistance of Au-NPs in PEDOT:PSS using hole-only devices (HODs). To investigate the correlation between current density and hole capture at the Au-NP trapping sites, HODs were fabricated with an ITO/capping layer/NPB (100 nm)/Al structure. Figure 5(a) presents the $J-V$ curve of the HODs for devices II, III, and IV for voltages of up to 8 V, while Figure 5(b) provides the $J-V$ curve of the HODs and the regional tendencies of the current transport mechanism up to 16 V. The HOD current densities can be divided into four parts:[24,25] ohmic, trap-filling space-charge-limited current (SCLC), trap-filled limit (TFL), and trap-free SCLC regions, according to the subsequent increase in operating voltage, as can be seen in Figure 5(b).[24,25] As Au-NPs were added into the PEDOT:PSS, the HOD current densities were decreased because of the occurrence of hole capturing at the Au-NP trapping sites in the trap-filling SCLC region, up to 9 V. However, after the TFL region, in the trap-free SCLC region, the tendency of the HOD current density to decrease was removed, meaning that the HODs with Au-NPs exhibited high current density values as the Au-NP concentration increased.

The current densities of all the HODs are dependent on the bias and the Au-NP density. Thus, the current density gradually decreases as the amount of Au-NPs increases in the capping layer in the trap-filling SCLC region, which may be due to an increase in the amount of impurities. This can be understood through the fact that charges accumulate at the Au-NPs as the electric bias increases. The carriers trapped by the Au-NPs induce poor current flow, which results from an increase in the trapping site density. Generally, the presence of trapping sites affects the charge carrier mobility (or transport) under SCLC conditions.[24,25] The enhancement of carrier mobility (density) at higher bias has been observed, which may be due to the field-

DOI: 10.1021/acsami.5b04248
ACS Appl. Mater. Interfaces 2015, 7, 15031−15041

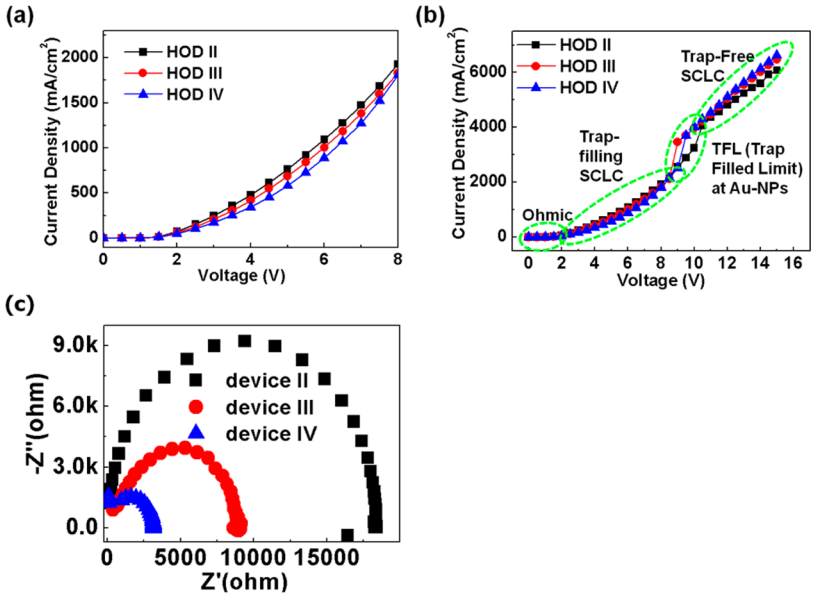

Figure 5. Hole-only devices for devices II, III, and IV at (a) low voltages, up to 8 V, and (b) whole voltages up to 16 V. The current-density region is divided into ohmic, trap-filling SCLC, TFL, and trap-free SCLC. (c) Cole−Cole plots and impedance data for devices II, III, and IV.

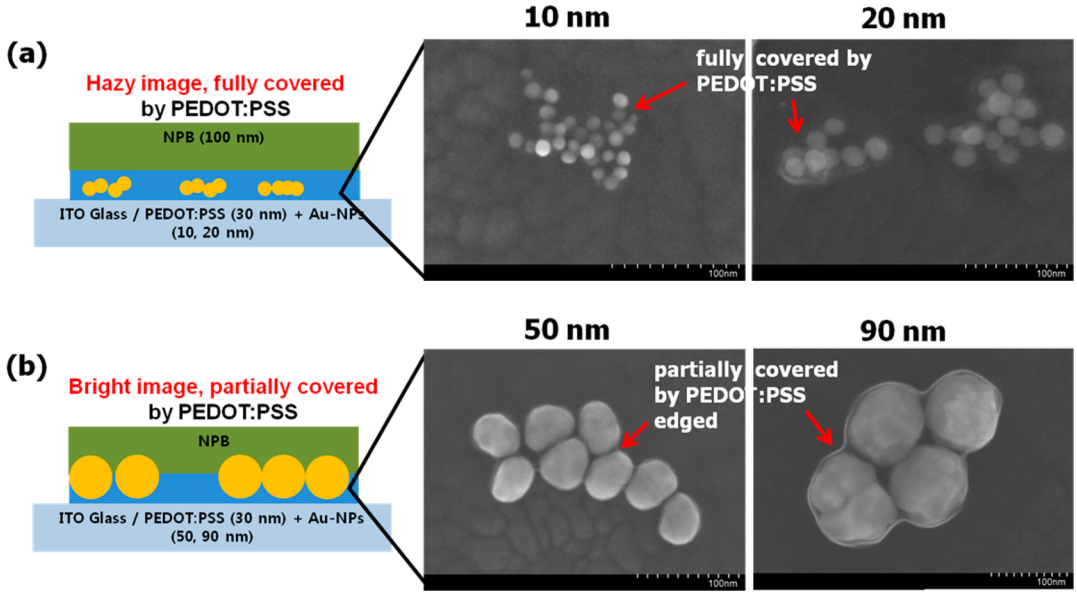

Figure 6. Schematic structures for different Au-NP sizes and degrees of vertical coverage between ITO and NPB HTL, respectively. (a) Hazy UHR FE-SEM images due to organic materials in conductive polymer for 10- and 20-nm Au-NPs in PEDOT:PSS. The Au-NPs were fully covered by the PEDOT:PSS. (b) Bright UHR FE-SEM images for 50- and 90-nm Au-NPs in PEDOT:PSS. The Au-NPs were partially covered by the PEDOT:PSS.

dependent lowering of hopping barriers. At high applied bias, this causes a gradual filling of the traps, and thus, the overall carrier mobility (density) increases with the electric field. This indicates that the SCLC behavior dominates the charge transport of the devices and the charges are accumulated at the interface between the HTL and EML. However, a quasi-ohmic transport was observed at high applied bias (over 10.5 V). This can be attributed to the fact that all of the traps are filled by the charges, leading to ohmic transport behavior.

1.5. Analysis of impedance spectroscopy (IS) measurements for Au-NPs in PEDOT:PSS. The effect of the PEDOT:PSS+Au-NP layers on the interfacial resistance between the ITO and the capping layer was evaluated to obtain insight into the hole trapping and current density under high-voltage conditions, using impedance spectroscopy (IS) measurements[14,15,26,27] as shown in Figure 5(c). IS is an outstanding, nondestructive tool for characterizing various optoelectronic devices, which can reveal charge-carrier lifetimes, electronic densities-of-states, and charge carrier concentrations.[14,15,26,27] Here, device II exhibited a higher interfacial resistance than the other devices, indicating that the PEDOT:PSS single layer was a severe bottleneck causing increased series resistance (R_s) with increased interfacial resistance between the ITO and NPB HTL layer. However, device IV exhibited reduced resistance at the ITO and capping layer interface, which improved its performance. This is consistent with the previous finding that the short-circuit current and power conversion efficiency in solar cells increase

DOI: 10.1021/acsami.5b04248
ACS Appl. Mater. Interfaces 2015, 7, 15031−15041

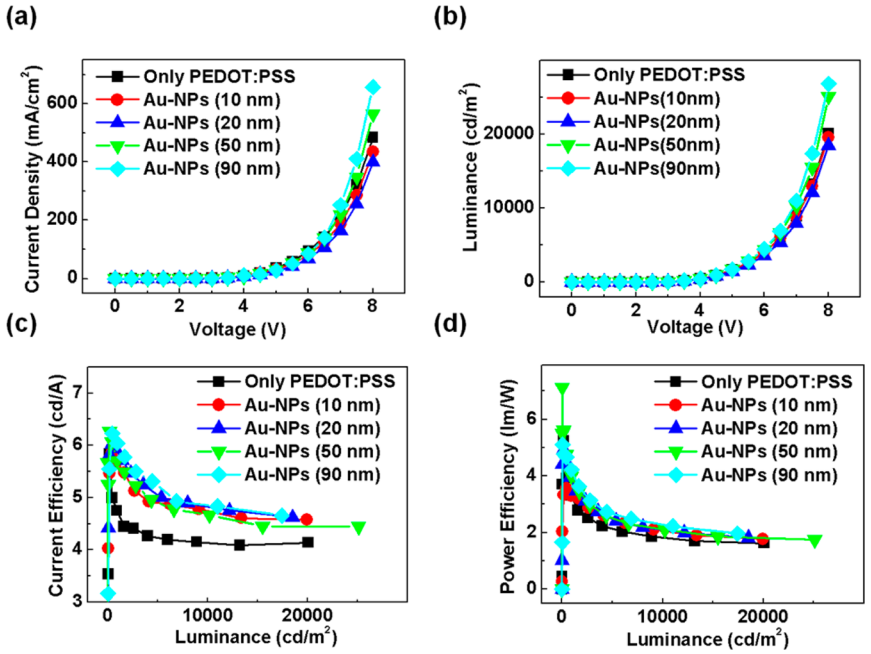

Figure 7. OLED characterization for 0-, 10-, 20-, 50-, and 90-nm Au NPs (different sizes and degrees of vertical coverage). The 0-nm case indicates that there were no Au-NPs in the PEDOT:PSS. (a) Current density vs voltage. (b) Luminance vs voltage. (c) Current efficiency vs luminance. (d) Power efficiency vs luminance.

with increasing impedance response, because the charge recombination is inhibited.[27] In addition, the current density in an OLED is generally determined by various parameters such as the interfacial resistance, the energy-level alignment with adjacent layers, and the trap centers. Although the current density at a lower voltage (approximately 8 V) in the trap-filling SCLC region does not correspond with the behavior of the interfacial resistance in this study, the behavior of the HOD current density at higher voltage in the trap-free SCLC region is well-matched with that of the interfacial resistance. Therefore, we might assume that the addition of Au-NPs to the PEDOT:PSS is favorable to the carrier mobility of both holes and electrons at higher voltage, inducing a small interfacial resistance. This can be attributed to the improved charge transport capability, and thus, the current flow between the ITO and the capping layer is increased after the traps are filled.[1−3] Based on the above discussion, it can be concluded that the HOD results are consistent with the impedance results, with the interfacial resistance of device IV being the lowest of all the examined devices.

2. Effects of vertical coverage of Au-NPs by PEDOT:PSS on device performance. *2.1. OLED device characterization for 0-, 10-, 20-, 50-, and 90-nm Au-NPs in PEDOT:PSS.* In order to investigate the effect of Au-NP size and the degree of vertical coverage within the PEDOT:PSS capping layer on the device performance (Figures 6(a) and (b)), additional devices were fabricated as follows. The device structure used was ITO/PEDOT:PSS+Au-NPs (0, 10, 20, 50, and 90 nm as the average Au-NP diameter)/Alq_3:C545T/Alq_3/LiF/Al. Note that no Au-NPs were present in the 0-nm Au-NP case. After deposition of the capping layer, the experimental procedures and conditions were identical to those used in the investigation of the effects of varying surface coverage.

The current density and luminance results for the devices with 0-, 10-, 20-, 50-, and 90-nm Au-NPs are shown in Figures 7(a) and (b), respectively. When Au-NPs with diameters smaller than the PEDOT:PSS thickness of 30 nm are enclosed in the PEDOT:PSS capping layer, both the current density and luminance are lower than those of the device with only PEDOT:PSS (device II). (Note that hazy images were observed during FE-SEM measurement in this case, due to the presence of organic materials, as shown in the inset of Figure 6(a). This means the Au-NPs were fully covered by the PEDOT:PSS.) However, in the case of large (50- and 90-nm) Au-NPs, both the current density and luminance are higher than those of the device with PEDOT:PSS only (device II). (Here, bright images of large Au-NPs with bordering PEDOT:PSS lines were clearly observed in the FE-SEM measurement, which were not due to organic materials. This means the Au-NPs were partially covered by the PEDOT:PSS, as shown in Figure 6(b).) Remarkably, the current efficiencies of all other devices (with both small and large Au-NPs) are higher than those of device II. This can be attributed to the fact that both the charge balance and the enhanced hole injection improve the device performance.

For the case of the surface coverage of the ITO without PEDOT:PSS (device I), the threshold with respect to the number of Au-NP trapping sites or the energy band alignment between the ITO electrode and the NPB HTL determines whether the carrier injection will be increased or decreased. With PEDOT:PSS enclosing the Au-NPs, certain Au-NP loading amounts can block the carrier injection and affect the total charge balance in the devices. However, as regards the vertical coverage, the size of the Au-NPs is the critical factor determining the current injection behavior. The EL intensity data and the absorption peaks of the pristine Au-NPs (10, 20, 50, 90 nm) in solution are shown in Figures S6(a) and (c), respectively. As the Au-NP size increased, a red-shift was induced in the UV spectra.[4−8,14,15] In Figure S6(b), the EL intensities of the examined devices were slightly enhanced at approximately 570 nm as the Au-NP size increased. The EL intensities at approximately 570 nm of the devices with small

DOI: 10.1021/acsami.5b04248
ACS Appl. Mater. Interfaces 2015, 7, 15031−15041

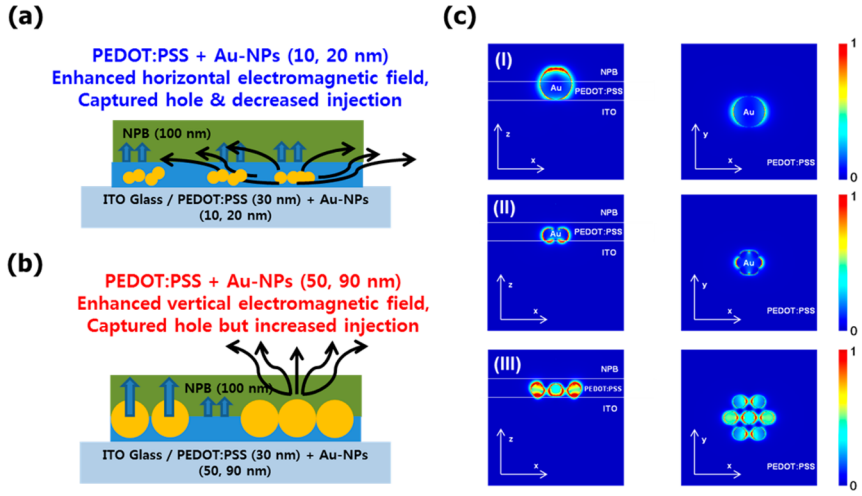

Figure 8. Light intensity modeling of structures with different degrees of coverage of Au-NPs by PEDOT:PSS. (a) 10- and 20-nm Au-NPs fully covered by PEDOT:PSS with enhanced horizontal electromagnetic field. (b) 50- and 90-nm Au-NPs partially covered by PEDOT:PSS with enhanced electromagnetic vertical field. (c) Electric field intensity distribution, $|E|^2$, in horizontal and vertical directions around Au-NPs simulated using the FDTD method. (I) 50-nm Au-NPs partially covered by PEDOT:PSS. (II) Clusters of 20-nm Au-NPs fully covered by PEDOT:PSS with a center-to-center distance between adjacent Au-NPs of approximately 10 nm. (III) A number of 20-nm Au-NP clusters fully covered by PEDOT:PSS with 30-nm center-to-center distance between the adjacent Au-NPs.

Au-NPs (10 and 20 nm) covered fully by the PEDOT:PSS were higher than those of the devices with large Au-NPs (50 and 90 nm), which were partially covered by the PEDOT:PSS. This could be due to the optical enhancement of the aggregated Au-NPs in the small number of stacked layers in the PEDOT:PSS. As the current densities are dependent on the Au-NP size, a perturbation in the recombination zone could also have occurred as a result of the microcavity effect.[19−21]

2.2. Finite-difference time-domain (FDTD) optical simulation for light intensity modeling of structures with different degrees of Au-NP coverage by PEDOT:PSS. To understand the different current density and luminance behaviors exhibited by the examined devices, extinction cross-sectional spectral models were simulated using the finite-difference time-domain (FDTD) method for each of the different device structures.[4−7,18] The spherical shapes of the Au-NPs can result in a high electric field and additional scattering directly above the Au-NPs,[4−7,18] which means that a higher current and luminance can be obtained compared to those of the control device without Au-NPs. Specifically, Au-NPs act like a current flow path for carriers in the PEDOT:PSS. Large Au-NPs (over 30 nm, which is the PEDOT:PSS thickness) that were partially covered by the PEDOT:PSS capping layer and that would come into direct contact with the NPB layer were used in the FDTD simulation. The electric field intensity was found to be enhanced in the vertical direction above the Au-NPs, as shown in Figures 8(b) and (c)-(I). This increased the current density and the number of excitons generated in the EML by increasing the number of hole carriers. However, when Au-NPs with sizes of less than 30 nm were considered, which would be fully covered by the capping layer, the electric field was found to be enhanced in the lateral direction of the Au-NPs, as shown in Figures 8(a) and (c)-(II). In this case, the electric fields might propagate along the lateral direction, because the Au-NPs would be fully covered by the PEDOT:PSS, which would cause additional carriers to be captured at the Au-NP sites. A simulation of the aggregated Au-NPs in the PEDOT:PSS was also conducted, as shown in Figure 8(c)-(III).

Electric field intensity distributions $|E|^2$ at plasmonic resonances were calculated in the horizontal and vertical directions around the Au-NPs, using the FDTD method. Incident light was excited from the top and surface plasmons at the Au-NPs in the 30-nm-thick PEDOT:PSS. In Figure 8(c)-(I), it is apparent that the 50-nm Au-NPs are partially covered, while, in Figure 8(c)-(II), the clusters of 20-nm Au-NPs are fully covered by the PEDOT:PSS. The center-to-center distance between adjacent Au-NPs is approximately 10 nm. In the case shown in Figure 8(c)-(III), a number of 20-nm Au-NP clusters are fully covered by PEDOT:PSS and the center-to-center distance between the adjacent Au-NPs is 30 nm. In addition, we performed additional FDTD simulations using 10-, 20-, 50-, and 90-nm Au-NPs, as shown in Figure S7. It was found that the electric field intensity distribution is strengthened when the diameter of the Au-NP is larger than the PEDOT:PSS thickness. The results of this simulation confirm the vertical coverage of the capping layer, which is in good agreement with the experimental results. The $|E|^2$ values of the 90-nm Au-NPs were significantly enhanced in the vertical direction above the Au-NPs, while those of the 50-nm Au-NPs were distributed in both the vertical and horizontal directions around the Au-NPs. This means that the vertical coverage of the Au-NPs by the PEDOT:PSS, which is dependent on the Au-NP size, can critically affect the current injection mechanism in fluorescent OLEDs.

The electric field was directed at random because the electrostatic interaction between the Au-NPs was generated in an aggregated cluster formation. According to the results of the FDTD simulation, Au-NPs with sizes of less than 30 nm that are not in direct contact with the NPB layer are very helpful in controlling the charge balance, as they decrease the current density and increase the number of excitons generated in the EML slightly. Therefore, we can conclude that the degree of vertical coverage of the Au-NPs, as determined by the particle size, is critical to judging the current injection behavior and to understanding the enhancement of the device performance when differently sized Au-NPs are incorporated in the PEDOT:PSS capping layer.

DOI: 10.1021/acsami.5b04248
ACS Appl. Mater. Interfaces 2015, 7, 15031−15041

CONCLUSIONS

In summary, we systemically investigated the effects of surface and vertical coverage of Au-NPs by PEDOT:PSS conducting polymer on device performance. It was found that optimized surface coverage of the Au-NPs enclosed within the PEDOT:PSS layer is beneficial to controlling hole injection. In particular, the device with an ITO/Au-NPs/Au-NPs +PEDOT:PSS structure exhibited the optimum performance, yielding improved charge balance and smaller interfacial resistance without the incorporation of the SPR effect. It can then be concluded that the addition of Au-NPs to PEDOT:PSS is favorable to the carrier mobility of both holes and electrons at higher voltage, as it induces small interfacial resistance. In addition, the current density behavior of HODs at higher voltage in the trap-free SCLC region is well-matched with that of the interfacial resistance.

The vertical coverage was determined by the sizes of the Au-NPs, with the Au-NPs being either partially covered or fully covered by the PEDOT:PSS, depending on their size. From the results of the FDTD simulation, full coverage of the Au-NPs by the PEDOT:PSS allowed the charge balance to be controlled more easily. This was due to a decrease in the current density and a slight increase in the number of excitons generated in the EML.

Therefore, the surface and vertical coverage of the Au-NPs in the capping layer, which is determined by the Au-NP loading amount and size, is critical to determining the current injection behavior and to understanding the resultant device performance enhancement.

ASSOCIATED CONTENT

Supporting Information

The optical density (OD) was estimated based on the absorption ratio for the capping layer with different Au-NP concentrations, and it was compared with that of the PEDOT:PSS layer without Au-NPs, as shown in Figure S1. Device structures I, II, IV, and V with different 10-nm Au-NP locations and degrees of surface coverage within PEDOT:PSS and between ITO and NPB are shown in Figure S2 (Insets: UHR FE-SEM images for devices I, IV, and V). The surface coverage calculation of the spin-coated Au-NPs (~10 nm in size) on the ITO glass was conducted using detailed UHR FE-SEM images, as shown in Figure S2. OLED characterization for different Au-NP positions and degrees of surface coverage for devices I and V [(a) current density vs voltage, (b) luminance vs voltage] are shown in Figure S3. The surface coverage calculation for 10-nm spin-coated Au-NPs on ITO glass (device I), based on a UHR FE-SEM image, is shown in Figure S4. The normalized EL intensities from 540−560 nm, with the magnified EL peaks depending on the different Au NP positions and degrees of surface coverage, are presented in Figure S5. The EL intensity data considering the vertical coverage and absorption peaks of the pristine Au-NPs (10, 20, 50, 90 nm) in solution are shown in Figures S6(a) and (c), respectively. The EL spectra of the devices with Au-NPs have a slightly enhanced shoulder peak at approximately 570 nm, which is caused by the presence of the Au-NPs, as shown in Figure S6(b). FDTD simulations for differently sized single Au-NPs in 30-nm-thick PEDOT:PSS are shown in Figure S7. The Au-NP diameters are (a) 10, (b) 20, (c) 50, and (d) 90 nm. The calculated electric field intensity distributions confirm the vertical coverage, as the diameters of the Au-NPs are larger than the PEDOT:PSS thickness. The Supporting Information is available free of charge on the ACS Publications website at DOI: 10.1021/acsami.5b04248.

AUTHOR INFORMATION

Corresponding Author

*Tel: +82-41-530-2295. E-mail: justie74@sunmoon.ac.kr.

Notes

The authors declare no competing financial interest.

ACKNOWLEDGMENTS

We express our hearty thanks to Mr. Jeeban Bastola for his valuable seminar throughout the progress of the work. This research was supported by the Basic Science Research Program through the National Research Foundation of Korea (NRF) funded by the Ministry of Education (Nos. 2014R1A1A2059762 and 2011-0014497) and the Industrial Strategic Technology Development Program (No. 10042412), funded by the Ministry of Knowledge Economy (MKE, Korea). H.-G.P. acknowledges support from an NRF grant, funded by the Korean government (MSIP) (No. 2009-0081565). T.J. acknowledges support from the Global Research Laboratory Program (2009-00439).

REFERENCES

(1) Kim, J. Y.; Hwang, C. R.; Jo, S. H.; Jung, W. G. Highly Clear Conductive Polymer Electrode Films Hybridized with Gold Nanoparticles. *Appl. Phys. Lett.* **2011**, *99*, 233304−1−23330433.

(2) Fujiki, A.; Uemura, T.; Zettsu, N.; Akai-Kasaya, M.; Saito, A.; Kuwahara, Y. Enhanced Fluorescence by Surface Plasmon Coupling of Au Nanoparticles in an Organic Electroluminescence Diode. *Appl. Phys. Lett.* **2010**, *96*, 043307−1−043307−3.

(3) Choulis, S. A.; Mathai, M. K.; Choong, V. E. Influence of Metallic Nanoparticles on the Performance of Organic Electrophosphorescence Devices. *Appl. Phys. Lett.* **2006**, *88*, 213503−1213503−3.

(4) Wang, D.; Yasui, K.; Ozawa, M.; Odoi, K.; Shimamura, S.; Fujita, K. Hole Injection Enhancement by Sparsely Dispersed Au Nanoparticles on Indium Tin Oxide Electrode in Organic Light Emitting Devices. *Appl. Phys. Lett.* **2013**, *102*, 023302−1−023302−3.

(5) Jesuraj, P. Justin; Jegannathan, K. Improved Hole Injection in Organic Light Emitting Devices by Gold Nanoparticles. *RSC Adv.* **2015**, *5*, 684−689.

(6) Kim, T. S.; Kang, H. B.; Jeong, S. J.; Kang, D. J.; Lee, C. Y.; Lee, C. H.; Seo, M. K.; Lee, J. Y.; Kim, B. J. Au@Polymer Core-Shell Nanoparticles for Simultaneously Enhancing Efficiency and Ambient Stability of Organic Optoelectronic Devices. *ACS Appl. Mater. Interfaces* **2014**, *6*, 16956−16965.

(7) Xiao, Y.; Yang, J. P.; Cheng, P. P.; Zhu, J. J.; Xu, Z. Q.; Deng, Y. H.; Lee, S. T.; Li, Y. Q.; Tang, J. X. Surface Plasmon-enhanced Electroluminescence in Organic Light-emitting Diodes Incorporating Au Nanoparticles. *Appl. Phys. Lett.* **2012**, *100*, 013308-1−013308-4.

(8) Shin, J. B.; Lee, S. M.; Kim, M. C.; Kim, D. H.; Jeon, D. Y.; Choi, K. C. Plasmonically Enhanced Optical Characteristics from Europium Organometallic Complex. *IEEE Photonic. Technol. L.* **2013**, *25*, 2342−2345.

(9) Schuller, J. A.; Barnard, E. S.; Cai, W.; Jun, Y. C.; White, J. S.; Brongersma, M. L. Plasmonics for Extreme Light Concentration and Manipulation. *Nat. Mater.* **2010**, *9*, 193−204.

(10) Atwater, H. A.; Polman, A. Plasmonics for Improved Photovoltaic Devices. *Nat. Mater.* **2010**, *9*, 205−213.

(11) Wu, J. L.; Chen, F. C.; Hsiao, Y. S.; Chien, F. C.; Chen, P.; Kuo, C. H.; Huang, M. H.; Hsu, C. S. Surface Plasmonic Effects of Metallic Nanoparticles on the Performance of Polymer Bulk Heterojunction Solar Cells. *ACS Nano* **2011**, *5*, 959−967.

DOI: 10.1021/acsami.5b04248
ACS Appl. Mater. Interfaces 2015, 7, 15031−15041

(12) Yang, J.; You, J.; Chen, C. C.; Hsu, W. C.; Tan, H. R.; Zhang, X. W.; Hong, Z.; Yang, Y. Plasmonic Polymer Tandem Solar Cell. *ACS Nano* **2011**, *5*, 6210−6217.
(13) Ji, W.; Zhao, H.; Yang, H.; Zhu, F. Y. Effect of coupling between excitons and gold nanoparticle surface plasmons on emission behavior of phosphorescent organic light-emitting diodes. *Org. Electron.* **2015**, *22*, 154−159.
(14) Yook, K. S.; Choi, M. S.; Kim, D. H.; Kim, C. S.; Song, M. K.; Kang, J. W.; Kwon, J. D.; Jeong, Y. S.; Nam, K. S.; Lee, S. H.; Jung, H. H.; Chung, K. B.; Bae, T. S.; Lee, J. Y.; Ryu, S. Y. Hydrogenated Amorphous Silicon Thin Film Solar Cells Using a Hybrid Buffer Layer of Gold Nanoparticle and Tungsten Oxide Thin Film. *ECS Solid State Lett.* **2012**, *1*, Q42−Q44.
(15) Jung, H. H.; Kim, D. H.; Kim, C. S.; Bae, T. S.; Chung, K. B.; Ryu, S. Y. Organic- Inorganic Hybrid Thin Film Solar Cells using Conducting Polymer and Gold Nanoparticles. *Appl. Phys. Lett.* **2013**, *102*, 183902−1−183902−5.
(16) Han, T. H.; Choi, M. R.; Woo, S. H.; Min, S. Y.; Lee, C. L.; Lee, T. W. Molecular Controlled Interfacial Layer Strategy Toward Highly Efficient Simple-Structured Organic Light-Emitting Diodes. *Adv. Mater.* **2012**, *24*, 1487−1493.
(17) Choi, W. J.; Kim, C. Z.; Kim, C. S.; Heo, W. S.; Joo, T. H.; Ryu, S. Y.; Kim, H. G.; Kim, H. J.; Kang, H. K.; Jo, S. J. A Repeatable Epitaxial Lift-Off Process from a Single GaAs Substrate for Low-Cost and High-Efficiency III-V Solar Cells. *Adv. Energy Mater.* **2014**, *4*, 1400589-1−1400589-6.
(18) Johnson, P. B.; Christy, R. W. Optical Constants of the Noble Metals. *Phys. Rev. B* **1972**, *6*, 4370−4379.
(19) Rhee, S. H.; Nam, K. B.; Kim, C. S.; Ryu, S. Y. Control of the Color Coordinates of Blue Phosphorescent Organic Light-Emitting Diodes by Emission Zone. *ECS Solid State Lett.* **2014**, *3*, R7−R10.
(20) Rhee, S. H.; Nam, K. B.; Kim, C. S.; Song, M. K.; Cho, W. S.; Jin, S. H.; Ryu, S. Y. Effects of Electron Mobility of the Electron Transport Layer on Fluorescent Organic Light-Emitting Diodes. *ECS Solid State Lett.* **2014**, *3*, R19−R22.
(21) Rhee, S. H.; Kim, C. S.; Song, M. K.; Chung, K. B.; Ryu, S. Y. Effects of Position of Exciton-Blocking Layer on Characteristics of Blue Phosphorescent Organic Light-Emitting Diodes. *ECS Solid State Lett.* **2014**, *3*, R49−R52.
(22) Bredas, J. L.; Norton, J. E.; Cornil, J.; Coropceanu, V. Molecular Understanding of Organic Solar Cells: The Challenges. *Acc. Chem. Res.* **2009**, *42*, 1691−1699.
(23) Pal, S. K.; Kesti, T.; Maiti, M.; Zhang, F. L.; Inganäs, O.; Hellström, S.; Andersson, M. R.; Oswald, F.; Langa, F.; Österman, T.; et al. Geminate Charge Recombination in Polymer/Fullerene Bulk Heterojunction Films and Implications for Solar Cell Function. *J. Am. Chem. Soc.* **2010**, *132*, 12440−12451.
(24) Burrows, P. E.; Shen, Z.; Bulovic, V.; McCarty, D. M.; Forrest, S. R. Relationship between Electroluminescence and Current Transport in Organic Heterojunction Light-emitting Devices. *J. Appl. Phys.* **1996**, *79*, 7991−8006.
(25) Kiy, M.; Losio, P.; Biaggio, I.; Koehler, M.; Tapponnier, A.; Günter, P. Observation of the Mott-Gurney Law in Tris (8-hydroxyquinoline) Aluminum Films. *Appl. Phys. Lett.* **2002**, *80*, 1198−1200.
(26) Kuwabara, T.; Kawahara, Y.; Yamaguchi, T.; Takahashi, K. Characterization of Inverted-Type Organic Solar Cells with a ZnO layer as the Electron Collection Electrode by ac Impedance Spectroscopy. *ACS Applied Mater. Inter.* **2009**, *1*, 2107−2110.
(27) Leever, B. J.; Bailey, C. A.; Marks, T. J.; Hersam, M. C.; Durstock, M. F. In Situ Characterization of Lifetime and Morphology in Operating Bulk Heterojunction Organic Photovoltaic Devices by Impedance Spectroscopy. *Adv. Energy Mater.* **2012**, *2*, 120−128.

DOI: 10.1021/acsami.5b04248
ACS Appl. Mater. Interfaces 2015, 7, 15031−15041